# 6: In-vivo experiments

This chapter presents the in-vivo DOT measurements which are central to this dissertation. The first rodent hemodynamic measurements performed with the time-encoded CW1 instrument are presented in Section 6.1. Although these initial measurements were important in showing that both [$HbO_2$] and [Hb] changes due to forepaw stimulation could be imaged with DOT , the frame rate of the CW1 imager was inadequate to capture all of the temporal features of the hemodynamic response. The development of CW4, a frequency-encoded imager capable of much faster frame rates, subsequently allowed the temporal hemodynamic response to electrical forepaw stimulation to be measured with DOT and quantitatively compared to similar measurements performed with functional MRI. The similarities and differences between DOT and fMRI measures of the blood oxygenation and volume time courses are then discussed with respect to currently accepted models for neuro-vascular coupling in Section 6.2.

## 6.1 CW DOT Measurements of Rodent Brain Function

Diffuse optical tomography (DOT) can image spatial variations in highly scattering optical media. We used an inexpensive and portable continuous-wave DOT system (CW1) to perform cortical absorption measurements on rodents following electrical forepaw stimulation. We present preliminary results showing that DOT is capable of quantitatively imaging both $HbO_2$ and Hb concentration changes during brain activation in a rat model. The results clearly demonstrate the capabilities of DOT as a noninvasive imaging modality.

### *Introduction*

Diffuse Optical Tomography offers the capability to simultaneously quantify the tissue concentration of both oxy- ($HbO_2$) and deoxyhemoglobin (Hb) [82-84]. Two or more near-infrared sources, with wavelengths specifically chosen to straddle the isosbestic point of the oxy/deoxyhemoglobin absorption spectrum, illuminate the tissue at various locations. The flux distribution at the tissue surface thus contains both spectral and spatial information about subsurface absorbers.

fMRI uses the paramagnetism of the Hb molecule to monitor metabolic activity through local changes in Hb, and thus blood oxygenation, hence the origin of the term BOLD (Blood Oxygen Level Dependent) imagery [42, 59, 95, 96]. fMRI offers millimeter spatial resolution, but only the relative quantity of Hb is measured. DOT can simultaneously image changes in total hemoglobin concentration (which relates to blood volume) and oxygen saturation ($HbO_2$/($HbO_2$+Hb)). One disadvantage of DOT is its limited spatial resolution, which leads to an intriguing possibility: the co-registration of simultaneously acquired DOT and functional MRI imagery, combining the spatial resolution of fMRI with the spectral discrimination of DOT [97, 98].

### *Background*

Ballistic photon imaging is usually performed in a shot noise-limited, photon-starved environment due to the low percentage of photons that actually penetrate the tissue unscattered. Thus the photon-counting detectors require only a modest dynamic range. Diffuse imaging, on the other hand, employs many sources and detectors distributed over a large region of illuminated tissue, so each detector may operate over an effective photon path length ratio in excess of 10:1. With total optode source-detector geometries spanning less than 1cm, as in rat brain studies, this effect is negligible, and the hardware can easily accommodate the 60-80dB of dynamic range required for rather good quality imagery.

On large subjects such as neonates or adult humans, however, optode dimensions of between 4 and 8cm are required. Under these conditions, that same photon path length ratio of 10:1 now translates into a flux attenuation range on the order of $10^6$:1! In order to obtain all the information available, each detector must be capable of operating over a 120dB dynamic range, which is rather large from an electronic perspective.

### *Preliminary validation of DOT via in-vivo measurement of rat brain function*

We developed a prototype portable diffuse imager (CW1) which can be used as a research tool for both characterizing tissue optical properties and guiding us toward future hardware and software design improvements. In order to evaluate the effectiveness of this design, we used this device to measure localized changes in cortical hemodynamics in response to a somatosensory evoked potential in an anesthetized rat.

In this study, electrical stimulation was applied to the median nerve within the forepaw. This is known to activate a volume of sensorimotor cortex within the parietal lobe. Any form of sensory stimulation (motor, tactile, visual, cognitive, etc.) produces a localized neuronal activation with a concomitant increase in metabolic rate. Because of flow-metabolism coupling, there is a localized increase in blood flow to fulfill the local increase metabolic demand for oxygen and glucose. The result is a localized increase in blood volume and, therefore, hemoglobin concentration. Because the increase in blood flow reduces the oxygen extraction fraction, hemoglobin saturation also increases. This is the basis for the MRI signal change associated with the BOLD response and has been explored with diffuse optical techniques by a number of investigators [99-102]. fMRI measurements of the spatial and temporal responses to electrical forepaw stimulation are shown in Figure 6.1 below.

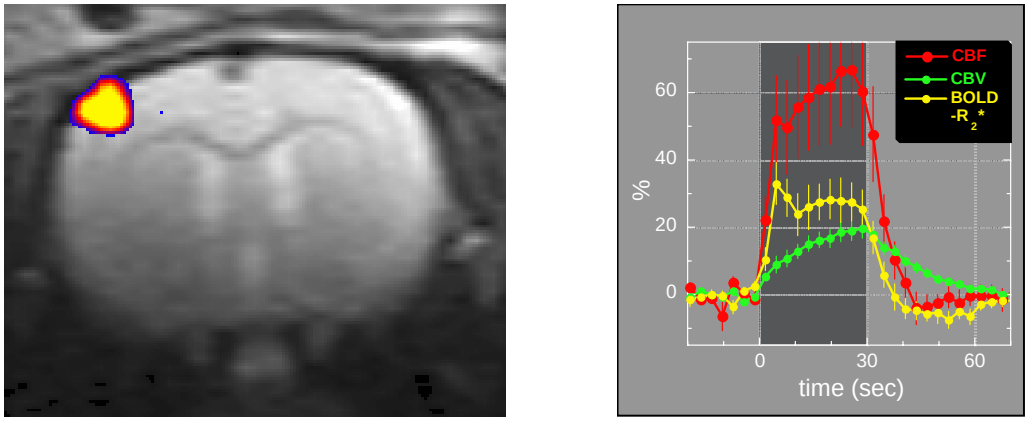


**Figure 6.1.** Images of the spatial and temporal responses to electrical forepaw stimulation measured with functional MRI.

### *Materials and Methods*

With approval of the Massachusetts General Hospital Subcommittee on Research Animal Care, a male Harlan Sprague Dawley rat (approx. weight 400 grams) was anesthetized with 1.5% halothane in oxygen for surgical preparation including insertion of femoral arterial and venous catheters and tracheotomy [16, 17, 24]. The rat was ventilated with a small fixed-volume mechanical ventilator (Harvard Apparatus) set to a tidal volume of 5cc throughout the experiment.

Following surgery, the halothane was discontinued and anesthesia was maintained with a 50 mg/kg intravenous bolus of alpha-chloralose followed by continuous intravenous infusion at 40 mg/kg/hr. In order to facilitate ventilation and to prevent muscular contractions from generating motion artifacts during stimulation, the rat was paralyzed with a 2mg/kg IV bolus of the nondepolarizing neuromuscular blocking agent pancuronium bromide, followed by continuous

intravenous infusion at 2 mg/kg/hr. Arterial blood pressure and rectal temperature were monitored throughout the experiment, and body temperature was maintained at 37.5 ± 0.5C by means of a thermostatic heating blanket. Arterial blood gases ($P_aO_2$, $P_aCO_2$ and pH) were determined from samples withdrawn through the arterial catheter, and ventilation was adjusted as needed to maintain normal arterial blood gas values.

Two 21 gauge bare copper wires were inserted just beneath the skin into the forepaw at the level of the carpal bones. Electrical stimulations were delivered as 5 volt rectangular pulses of 0.2msec duration at a 3 Hz repetition rate. Prior to paralysis, this voltage was determined to be at least 2.5 times the level at which a muscular twitch response was generated.

The head was secured in a stereotactic headframe (Kopf Instruments) both to reduce motion artifacts and to serve as a mechanical support for a three-axis translation stage used to position the optode assembly directly against the scalp. The stimulation protocol began with acquisition of a baseline image followed by a 45-second period of stimulation, during which an image was acquired every 5 seconds. After stimulation was discontinued, images were collected every 5 seconds for an additional 60 seconds. All stimulations were performed at least 45 minutes after discontinuation of the halothane in order to minimize any residual hemodynamic effects.

The optode arrangement is shown in Figure 6.2. The 9 source fibers were arranged in a 3 x 3 grid with a 3 x 5 mm spacing. The 16 collection fibers were arranged in a 4 x 4 grid with the same 3 x 5 mm spacing. To improve optical coupling, the height of each fiber was manually adjusted to match the surface contours of the skull. The Z-positions were not measured, nor was the actual contour of the scalp. The images were reconstructed with the assumption that the scalp contour was flat and that the scalp, skull, cerebral spinal fluid, and brain system could be treated as a homogeneous, semi-infinite medium, except for the localized activation. Images were reconstructed in a 9 x 15 mm plane positioned at a depth of 4 mm, with a thickness of 1 mm, and located parallel to the source/detector plane. The voxel size was 0.45 x 0.75 x 1 mm. With this geometry, we only reconstruct 2D images and we assume that the out-of-plane optical properties remain unchanged. This means that any out-of-plane optical changes that do occur are projected into the image plane. Our reconstructions were performed using 10 iterations of the SIRT algorithm, starting with an initial guess of zero perturbation [103, 104]. It was critical to phase-lock the image sequence with the respiration rate to minimize the physiologic interference due to periodic changes in venous volume due to positive pressure mechanical ventilation.

The results are presented here as an average of 6 trials on a single rat. Figure 6.2 shows the results of a 45-second electrical stimulation to the right forepaw. The baseline image is shown at 0 seconds as well as the peak activation image at the end of the 45-second stimulation, followed by a return to the baseline image at 95 seconds. The images reveal an increase in absorption in the left hemisphere. A greater increase in absorption was seen at 830nm compared to 780nm. This is consistent with the standard vascular response of increased blood volume and oxygen saturation.

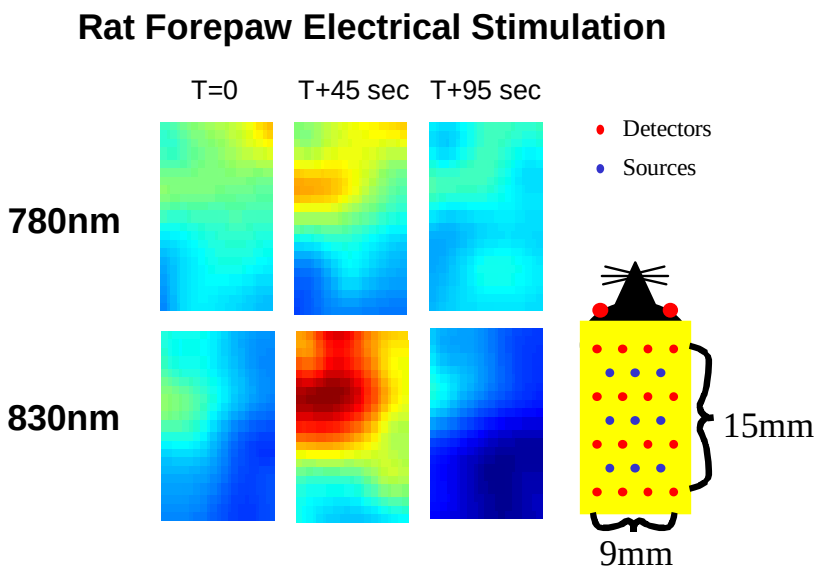


**Figure 6.2.** DOT images of rat brain function at the peak response following 45 seconds of electrical stimulation to the right forepaw. The recovery to baseline is shown 50 seconds after cessation of stimulation.

***Summary***

Diffuse optical tomography (DOT) can image spatial variations in highly scattering media, and offers great promise as an adjunct to fMRI for simultaneous real-time quantification of total hemoglobin concentration and oxygen saturation. We discussed a number of issues that influence the design and development of diffuse imaging instrumentation. We then described the use of a prototype CW DOT imager to acquire DOT images of rat brain function following forepaw stimulation. These DOT images qualitatively agree with the expected vascular response to neuronal activation. In particular, our measured absorption changes are consistent with the standard observation of an increase in blood volume and oxygen saturation.

## 6.2 Temporal comparison of DOT and fMRI in rodent somatosensory cortex during forepaw stimulation

The main purpose of these measurements was to quantitatively compare the temporal evolution of the cerebral hemodynamic response as measured with functional Magnetic Resonance Imaging (fMRI) and Diffuse Optical Tomography (DOT). Other researchers have observed qualitative spatial [19-21] and temporal [22] correspondence between the fMRI Blood Oxygen Level Dependent (BOLD) signal and diffuse optical measures of deoxyhemoglobin ([Hb]) and oxyhemoglobin ([$HbO_2$]) concentrations in humans, however to date there has been no quantitative examination of the temporal correlation between fMRI and DOT. Previous measurements of rat somatosensory cortex have revealed much about the time course and spatial extent of Cerebral Plasma Volume (CPV) and BOLD signals following median nerve stimulation in a rodent model [12, 16, 17, 24-27]. Since this preparation has been well characterized with fMRI, we chose it as a convenient model to cross-validate fMRI and DOT. Since the forepaw stimuli were easily varied, we also sought to explore the effects of stimulus repetition rate, duration, and magnitude, both to determine the robustness of this preparation and to explore the physiology underlying the neurovascular response.

### 6.2.1 Background

fMRI has led to significant advances in neuroimaging during the last 10 years [2, 105, 106]. It allows near real-time observation of the hemodynamic response to neuronal activation. The BOLD fMRI signal scales approximately with absolute changes in deoxyhemoglobin concentration ([HbR]), however questions remain about the exact relationship between the BOLD signal and the vascular response. Likewise the coupling between neural activity and the vascular response itself is poorly understood [107, 108]. Since MRI and DOT are based upon different fundamental principles, cross-validation can help us to better understand both the neurophysiology behind cortical activation and the biophysics behind the measurement techniques themselves.

In this study, we compare fMRI and DOT measurements of the temporal evolution of the hemodynamic response to electrical forepaw stimulation in rat somatosensory cortex. DOT is a noninvasive neuroimaging technique which exploits both the spectrally varying absorption and diffuse scattering nature of near-infrared light propagation through tissue [99, 109, 110]. Unlike fMRI, DOT can directly and simultaneously measure concentration changes in deoxyhemoglobin ([Hb]), oxyhemoglobin ([$HbO_2$]), and total hemoglobin ([HbT] = [Hb] + [$HbO_2$]) in cortical tissue.

### 6.2.2 Materials and Methods

#### *Anesthesia*

Male HSD rats of weight 300-400g were anesthetized with ~1.8% isoflurane vapor in oxygen enriched (60-80% $O_2$) air. A core temperature of 36.7+/-0.5'C was maintained during the course of the experiment using a laminar heater (Watlow Corp.) placed under the ribcage and upper abdomen. The rat was tracheotomized and mechanically ventilated with a custom-designed ventilator using patient-triggered inspiration protected by a time-triggered backup. The ventilator operated in assist-control mode, with a peak inspiratory pressure (Paw + tubing drop) of 15cm$H_2O$ and an inspiratory trigger threshold of between –2 and –5cm$H_2O$, which was adjusted as needed to maintain a nominal et$CO_2$ of 38+/-5 Torr. Both were adjusted as needed to maintain adequate ventilation during the experiment. The nominal respiration rate was around 40 BPM.

Following tracheotomy, both venous and arterial catheters, each consisting of a 12" length of PE-10 tubing secured to a luer hub, were placed into the right femoral vessels. After catheterization, a loading dose of 50mg/kg of $\alpha$-chloralose in saline was administered followed by a continuous venous infusion of between 30 and 45mg/kg/hr, titrated to stabilize the MAP at 100+/-10 mmHg. The MAP was monitored through the arterial line using a piezoresistive strain gauge sensor (Utah Medical "Deltran" series). The isoflurane concentration was then reduced to ~0.4% to provide some residual analgesia, during which time the rat was placed in a stereotactic headframe and the optode assembly was lowered onto the scalp. Once this had been achieved, the isoflurane was discontinued and the stimulator and ECG monitor electrodes were inserted. Our trials began after a one hour washout period on $\alpha$-chloralose alone to eliminate any residual hemodynamic effects from the isoflurane. During this time the infusion rate was adjusted to maintain a nominal MAP of 100 mm.

#### *Biomonitoring*

The isoflurane, oxygen, and end-tidal $CO_2$ concentration were measured with a Datex Capnomac anesthesia monitor. A passive accumulator within the expiratory limb of the ventilator compensated for the small (~3-5ml) tidal volumes. The accumulator consisted of a tee fitting in series with the Capnomac sampling line to which the empty barrel of a 3cc syringe was attached. This provided no additional obstruction or backpressure yet offered up to 3ml of storage volume in which the exhaled breath could accumulate prior to sampling.

The ECG signal was recorded through electrodes fashioned from standard 27 gauge tuberculin needles, cleaned with isopropanol to remove the silicone lubricant normally applied by the manufacturer to reduce the discomfort of needle entry. The two sensing needles were then inserted through skin folds above each shoulder blade, and contact to the ECG preamplifier was made using alligator clips clamped near the protruding end of the needle. A ground needle was inserted along the midline about 1cm rostral of the tail. The luer hub prevented the needles from exiting the skin. Clean ECG signals with a clearly discernable QRS interval were obtained. The mean arterial pressure was monitored using a commercial piezoresistive blood pressure transducer (Utah Medical Deltran series) operated in direct current mode. The amplifier gain was calibrated to provide a 1Volt output with a static water column of 136cm (equivalent to 100 mmHg).

### *Stimulation*

All stimulation was controlled by a PC computer through a digital I/O card, which drove a custom-built stimulus isolation unit equipped with a current delivery monitor. 27 gauge hypodermic needles, prepared as discussed above, served as stimulus electrodes. The stimulator produced an inductively-coupled signal which provided galvanic isolation to minimize electrode polarization. Prior measurements with this stimulator delivering 200us pulses at currents below ~2 mA have shown that the electrode-tissue interface remained stable, with current drift below 5% over an 8 hour period. Our pulsewidths were fixed at 200us and the stimulus current ranged from 500uA to 2mA. The temporal data shown here was collected using two stimulus paradigms, both with 2mA stimulus pulses at a rate of 3Hz:

* 6 second stimulus duration (18 pulses) followed by a 54 second recovery.
* 30 second stimulus duration (90 pulses) followed by a 90 second recovery.

The stimulus paradigms used in this study were chosen to mirror those used in the fMRI time course measurements. The short stimulus duration (6 sec) was originally selected to provide just enough time for the BOLD response to reach a maximum value, in order to enable the large amount of averaging necessary to investigate small potential transient features like the BOLD 'initial dip' [17]. The longer stimulus duration (30 sec) was selected to enable the CPV response to almost reach a maximal response, while avoiding the progressive attenuation that is seen for stimuli of longer durations [111]. Delivery was confirmed with a dynamic current monitor circuit, which permitted real-time observation of the current delivered for each stimulus pulse in the train.

### *DOT Instrumentation*

We used a "continuous-wave" diffuse optical tomography system with an optode assembly consisting of 9 pairs of collocated dual-wavelength (690nm and 830nm) fiber-coupled laser diode sources and 16 fiber-coupled silicon APD detectors. Each source was square-wave amplitude-modulated at a single frequency between 4kHz and 8kHz with a frequency spacing of 200Hz. The outputs from each of the 16 APD detector modules were AC-coupled and amplified as needed before being sampled by a 16 bit ADC at a rate of about 40ksps. The resulting data files were stored on an 80GB hard disk drive for post-processing.

A diagram of the optode assembly is shown in Figure 6.3. All of the sources and detectors were coupled through 200um polymer-clad silica fiber (3M FT-200-URT) to a 1" x 1" x 0.125" thick pliable rubber pad through which the 9 pairs of source fibers and the 16 detector fibers were inserted in a standard "9 within 16" interlaced grid pattern. The row and column spacing was fixed at 0.2" using a piece of G-10 perfboard as a template to mark the fiber insertion points. This yielded a minimum source-detector spacing of 0.14" (3.6mm) and a total grid size of about 0.6" (15mm) square. This source-detector spacing was large enough to provide an adequate spatial reconstruction using the methods described below [112]. The optode pad was anchored at its four corners and spaced about

1.5” below an aluminum support plate using flexible steel tubing. This design offered a significant degree of compliance which kept the fiber ends normal while allowing the pad and steel tubing to flex to follow the contours of the skull.

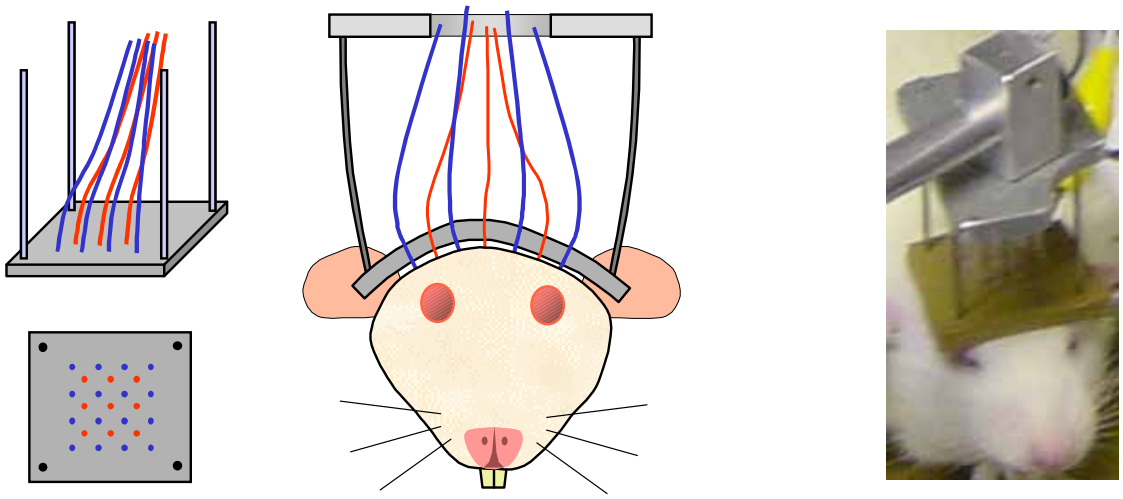

**Figure 6.3.** A sketch of the transcutaneous cortical optode assembly and a photo showing its placement. The 9 source fibers (red) are surrounded by 16 detector fibers (blue). Both the rubber pad and steel support tubing flexed, allowing individual optodes to remain normal to the surface while the entire assembly conformed to the curvature of the scalp.

### *Data Processing and Image Reconstruction*

Our raw datafiles were acquired continuously, and consisted of consecutively digitized voltage samples from each of the 16 detector channels at a cyclic collection rate of about 40ksps for a period of 8 minutes. This yielded a two-dimensional array of dimension 16 (detectors) x n (time points), where n was around 19.2 million for an 8 minute collection. The first processing step was to bandpass filter the data using a sharp multi-pole filter algorithm to extract the individual source signals while minimizing the adjacent channel crosstalk. The result of this step was a much smaller 3-D array of dimension 16 (detectors) x 18 (sources) x m (time points), where m was now only 4.8k (10 frames/sec over 8 minutes). These files were further down sampled to 2 frames/second with a 1 second time constant low pass filter.

Each 8 minute datafile consisted of either 4 or 8 identical trials. The trials within each datafile were then block averaged to reduce the impact of biogenic noise, using the stimulus onset time of each trial for synchronization. The short (~15 sec) prestimulus period was used to establish an absorbance baseline.

During these experiments, the mechanical ventilator was patient-triggered. The natural variability of patient-triggered ventilation (as opposed to the fixed cycle rate of time-triggered ventilation) led to a greater decorrelation of, and hence more immunity to, the hemomodulating effects of both heartbeat and respiration.

Our voxellation region for image reconstruction consisted of a 40 x 40 pixel two-dimensional slice, which corresponded to a 2 x 2 cm area at a depth of 2mm, from which the actual imagery only represented the central 1 x 1 cm portion of this region.

For image reconstructions of spatially varying optical properties, we employed a standard linear approach known as the Rytov approximation, $\Phi = \Phi_o \exp(\Phi_{scat})$ [113]. The total fluence $\Phi$ consists of a background field, $\Phi_o$, that depends on background optical properties, and a perturbed field, $\Phi_{scat}$, which is linearly related to a set of spatial variations in the optical absorption coefficient $\delta\mu_a$. We discretized

the integral into cubic voxels ($h^3$) and wrote the Rytov approximation as **y=Ax** by making the following associations:

$$y_i = \ln\left[\frac{\Phi(\mathbf{r}_{s,i}, \mathbf{r}_{d,i})}{\Phi_o(\mathbf{r}_{s,i}, \mathbf{r}_{d,i})}\right], \qquad A_{i,j} = -\frac{vh^3}{D_o}\frac{G(\mathbf{r}_{s,i}, \mathbf{r}_j)G(\mathbf{r}_j, \mathbf{r}_{d,i})}{G(\mathbf{r}_{s,i}, \mathbf{r}_{d,i})} \quad \text{and} \quad x_j = \delta\mu_{a,j}$$

Here**,** $\mathbf{r}_s$ and $\mathbf{r}_d$ are the position of the source and detector respectively; *G* is the Greens function of the photon diffusion equation for given background optical properties, and a semi-infinite geometry with extrapolated zero boundary conditions. The subscripts **i** and **j** represent the indices of each source-detector pair and the indices of each voxel, respectively. The inverse problem was then solved using the (Tikhonov regularized) Moore-Penrose generalized inverse, $\mathbf{x} = \mathbf{A}^T(\mathbf{A}\,\mathbf{A}^T + \lambda I)^{-1}\mathbf{y}_{\text{meas}}$, where *I* is the identity matrix [114]. We then use a spectroscopic analysis at each voxel to calculate the corresponding [$HbO_2$] and [HbR] changes [115, 116].

The activation volume, as measured with fMRI, was approximately 2mm FWHM [12]. The spatial resolution of the fMRI measurements was approximately $0.6mm^3$, and the fMRI data were integrated within a $3mm^3$ sample volume for the time course calculation. For DOT, the voxel size was $0.5mm^3$ and the optical point spread function in the lateral dimension was approximately 2.8 $mm^2$, with a constrained vertical depth of 1mm centered at a depth of 1.5mm. Since our voxel spacing met the Nyquist criterion, the optical point spread function limited the spatial resolution of our imagery, and thus defined the sample volume for our time course calculations. The value of λ, (the regularization constant), was chosen to provide a balance between image noise and resolution, as determined by evaluating the contrast to noise ratio [117]. This value was kept fixed across all rats, and corresponded to a PSF at the image center with a FWHM of 2.8 mm [53, 118].

### 6.2.3 Results

A typical spatially resolved image for a single rat is shown in Figure 6.4. Based upon such spatial maps, the individual DOT time courses were extracted from the region of maximal activation, elicited by electrical forepaw stimulation using the 6 and 30 second stimulus paradigms described earlier. The individual [HbR], [$HbO_2$], and [HbT] time courses from five rats were first normalized and then group-averaged, using the stimulus onset time for synchronization. A plot of the relative magnitudes of these time courses is shown in Figure 6.5.

Shown for comparison are CBV and BOLD results from fMRI data collected under similar conditions. Figure 6.6 shows the group-averaged temporal evolution of DOT [HbR] and [$HbO_2$] plotted with the fMRI BOLD signal, and DOT [HbT] plotted with the fMRI cerebral plasma volume (CPV). Since the differences in the fMRI datasets collected at 2.0T and 4.7T were not statistically significant, the curves for all but the 6 second CPV dataset (which was measured at 2.0T only) show the averaged results of the datasets collected at both 2.0T and 4.7T field strengths [24].

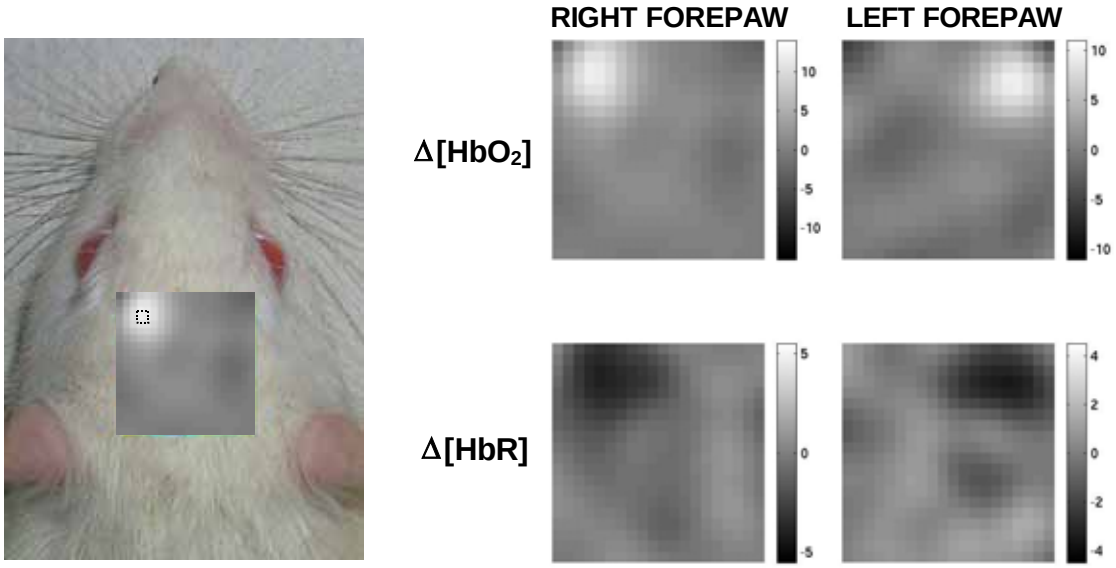


**Figure 6.4.** Spatially resolved DOT images from a single rat showing contralateral activation of the somatosensory cortex. The dashed square indicates the pixel showing maximal activation, from which the time courses would be obtained.

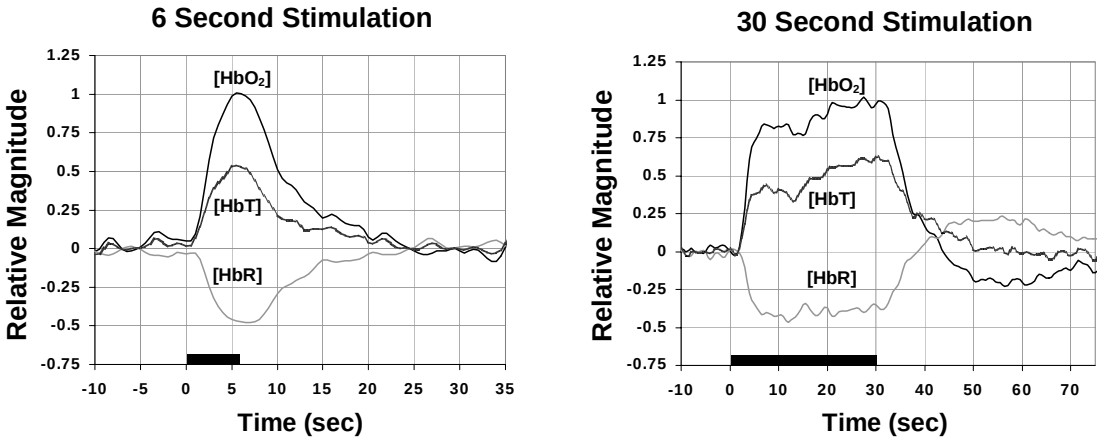


**Figure 6.5.** DOT time courses at 3Hz stimulation for both 6 and 30 seconds, showing the relative magnitudes of [HbR], [$HbO_2$], and [HbT]. The transient increase in [$HbO_2$] is greater than the corresponding decrease in [HbR], leading to a net increase in [HbT] following stimulation. The black bars represent the duration of stimulation, and uncertainty is shown by the error bars in Figure 6.6 which presents this data in greater detail.

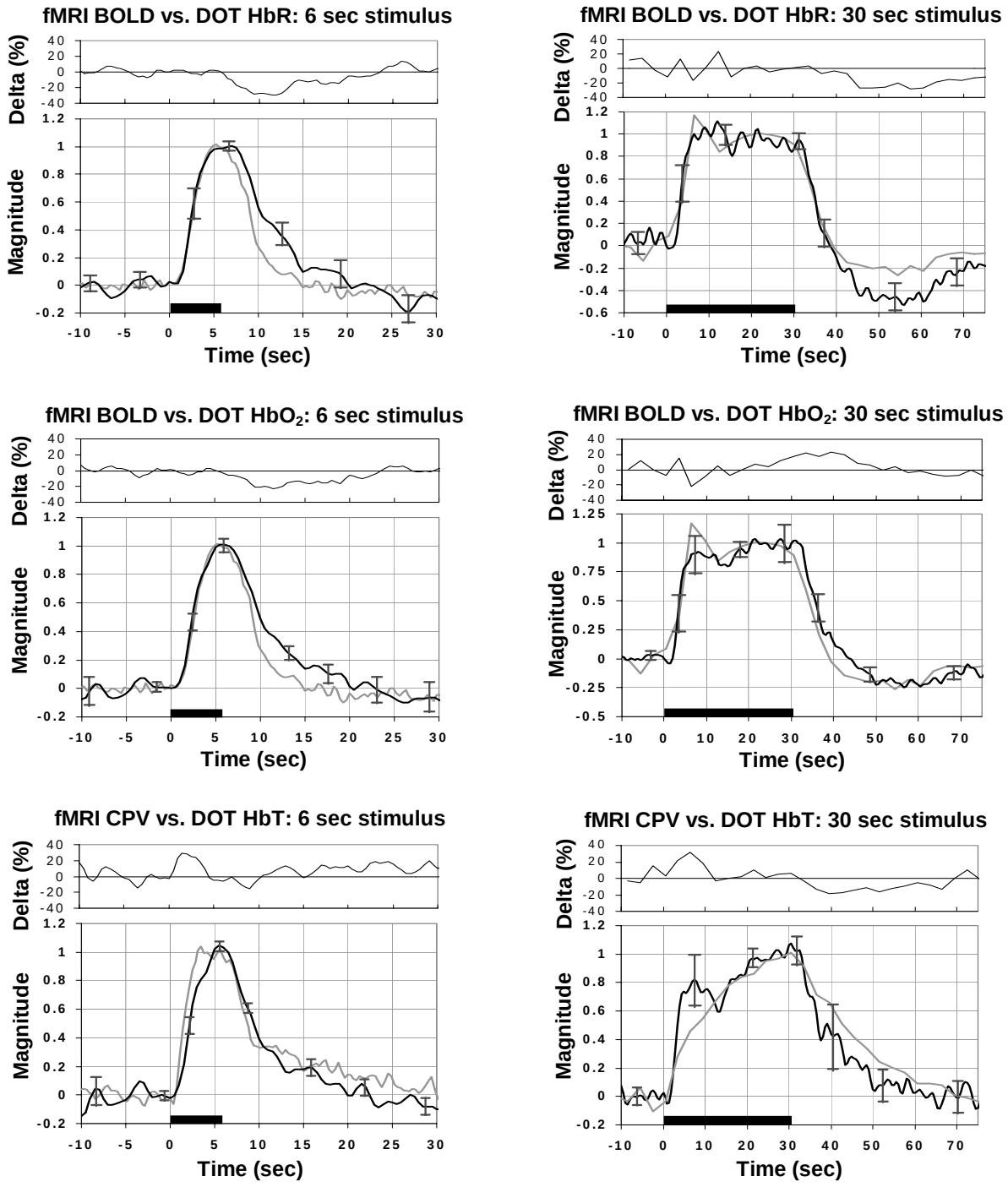


**Figure 6.6.** The temporal evolution of cerebral blood volume and hemoglobin concentration, as measured with fMRI (gray curves) and DOT (black curves) at a forepaw stimulus current of 2mA. Error bars are shown for the DOT data, and fMRI/DOT delta vs. time curves are shown above each plot. Uncertainty in the fMRI data is comparable [17, 24]. The fMRI curves (except for the 6 second CPV dataset, measured at 2.0T only) show the average of data collected at both 2.0T and 4.7T.

The plots in Figure 6.7 show the effect of several stimulus parameters on the DOT [$HbO_2$] response. Since the [$HbO_2$] and [HbR] responses were similar in shape (albeit opposite in direction),

only the larger [$HbO_2$] response is shown. Each plot consists of the contiguously collected data from two rats.

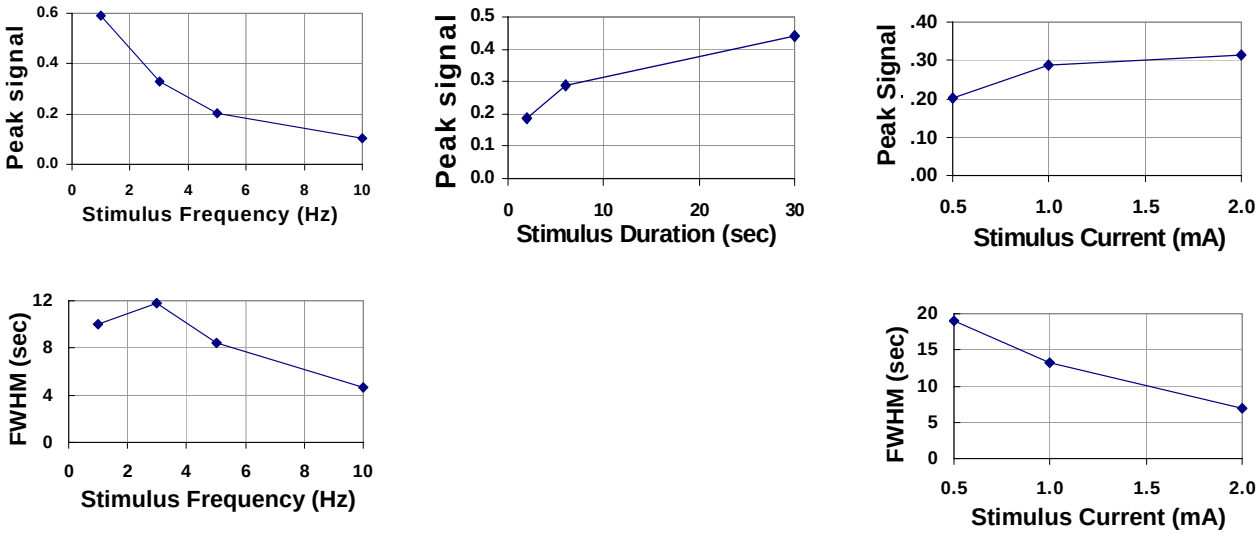


**Figure 6.7.** [$HbO_2$] peak signal magnitude and FWHM (in arbitrary units) vs. stimulus frequency, current, and duration. Unless otherwise noted, the nominal test conditions were: $F_{stim}$ = 3Hz, $I_{stim}$ = 1.0mA, $T_{stim}$ = 6 sec. See text for details.

## 6.2.4 Discussion

DOT and fMRI provide similar measures of hemodynamic activity. Both employ hemoglobin as an endogenous contrast agent, however there are significant differences in how it is actually detected. They also differ in how they measure cerebral blood volume. Although the detection mechanisms of DOT and fMRI differ and sensitivity varies with vessel diameter for both methods, they may still provide similar temporal information if their vascular weighting functions are comparable [119].

### *Vascular sensitivity of fMRI and DOT*

Because [HbR] is a paramagnetic contrast agent for MRI, BOLD fMRI detects local magnetic field perturbations produced by absolute changes in [HbR] within each voxel. Since $HbO_2$ is diamagnetic like surrounding tissue, it has minimal influence on proton precession and thus cannot be measured with fMRI. Cerebral plasma volume was measured with the aid of MION, an exogenous superparamagnetic contrast agent, yielding a signal proportional to the change in total plasma volume fraction within each voxel [16].

DOT detects changes in [HbR] and [$HbO_2$] by measuring their effect on the optical absorption properties within the tissue. Measurements at multiple source wavelengths allow the relative contributions of each component to be calculated independently. Thus DOT can measure changes in [HbR], [$HbO_2$], and [HbT] simultaneously, without the need for exogenous contrast agents. The DOT voxel locations were chosen for analysis based upon the maximum HbT response. HbT provided better spatial localization than HbR because the locus of the HbR signal shifted with time as HbR-rich blood presumably traversed the local draining veins.

DOT is subject to its own concerns and limitations. As the image reconstruction process is ill-posed, it can lead to errors in the hemodynamic characterization. In an effort to reduce both spatial and [Hb] estimation errors, we chose optical sources centered at 690nm and 830nm, since it is believed that a source wavelength of 690nm is preferable to 780nm when paired with an 830nm source for DOT [1,

120]. Also, features with high absorbance, such as large blood vessels, can absorb nearly all of the local incident flux, thus reducing DOT signal sensitivity in these areas. Thus, most DOT measurements are uniformly sensitive to vessels smaller than the optical absorption length, with sensitivity progressively decreasing for larger vessels [18].

### *Comparison of the hemodynamic response functions*

The data in Figure 6.5 show the typical hemodynamic response pattern, with an event-related increase in [$HbO_2$] accompanied by a smaller decrease in [HbR]. The hemodynamic responses following both 6 and 30 second stimulation were delayed approximately 2 seconds from stimulus onset, which is consistent with similar human studies. Following stimulus onset, the [$HbO_2$] and [HbT] both peaked at ~5 seconds and the [HbR] peaked at ~7 seconds, which has also been seen in humans [121, 122]. Unlike those studies, which observed a ~1 second difference between the onset of the $HbO_2$ and HbR responses, the rise in [$HbO_2$] nearly coincided with the fall in [HbR] in both the 6 and 30 second data. This might be due to the shorter cerebral mean transit time in rats as compared to humans. In whisker barrel cortex, some have seen similar results [123], while others observed the change in [$HbO_2$] leading [HbR] by about 1 second [124].

For the 30 second stimulus, the data show a post-stimulus overshoot in [HbR] and undershoot in [$HbO_2$], both of which slowly returned from their peak values to baseline after ~ 30 seconds. The [HbT] did not exhibit any undershoot, however, and returned to baseline within ~20 seconds of cessation of stimulation. The hemodynamics following the 6 second stimulus did not exhibit any under- or overshoot, which is presumably due to the brevity of the stimulus in relation to the length of time required to achieve vascular delayed compliance [25].

Although there is an overall scale factor between DOT and fMRI data, signals normalized to the main response can be compared for similarity in the post-stimulus region. The DOT [HbT] time courses followed the 6 and 30 second fMRI CPV time courses reasonably well, showing similar profiles in both cases. In principle, both modalities should exhibit near linear proportionality to changes in the blood volume fraction, provided that the hematocrit within the region of activation remains constant during the measurement [12, 125]. However it is possible that blood plasma volume (and thus hematocrit) may vary following cerebral activation, though this has not yet been confirmed [123]. If so, then this could introduce nonlinearities in both the DOT [HbT] and fMRI CPV responses. The DOT [HbT] response showed a rapid initial rise to a transient peak about 5 seconds after stimulus onset, followed by a later slow rise. Using rapid sampling, fMRI data also showed this multi-phasic response in blood plasma volume (Mandeville et al. 1999b). Although the transient peak observed in the DOT [HbT] data was not present in the averaged fMRI data, it was observed in individual rats. Also interesting is a similar transient peak in estimated $CMRO_2$ following whisker barrel stimulation at 1.6mA [123].

The DOT [HbR] and [$HbO_2$] 30 second time courses both tracked the fMRI BOLD time course within the stimulus region, but their behavior in the post-stimulus region differed. [HbR] showed a more pronounced undershoot than either [$HbO_2$] or BOLD, although its contour (i.e. the shape of the curve) matched the BOLD signal very closely. The [$HbO_2$] tracked the BOLD signal better in magnitude than did [HbR], but the contours of the two time courses appeared to differ. Although [HbR] and BOLD signal in the post-stimulus region cannot be shown to differ statistically given the variability between animals, as reflected by the error bars in Figure 6.6, there are several potential sources of discrepancy between the two modalities. The most likely of these are:

1. BOLD fMRI includes contributions from intravascular blood water, as well as extravascular water that is influenced by gradients extending from the blood vessels. The latter effect is expected be roughly linear with [HbR], while the former effect is most pronounced at low

fields [126] and diminishes at higher field strengths [127]. Elevated blood volume ([HbT] and CPV) in the post-stimulus region should produce a negative effect on both HbR and extravascular BOLD signal, whereas elevated blood water will increase intravascular BOLD signal at low fields due to the longer T2 of blood relative to parenchyma. For this reason, high-field BOLD signal should more closely reflect [HbR] in the post-stimulus region if the source of the post-stimulus undershoot is elevated CBV. In fact, the BOLD post-stimulus undershoot in the 4.7 Tesla data was observed to be larger than that in the 2 Tesla data [24], consistent with this explanation.

2. DOT and fMRI undoubtedly sample the activated volume with different sensitivity profiles, particularly with respect to depth from the cortical surface. Since the temporal evolution of the cerebral hemodynamic response is influenced by the arterial, capillary, and venous compartments, fMRI and DOT are likely governed by different weightings of these three vascular compartments.

### *Significance of [$HbO_2$] undershoot*

Based upon the fMRI measurements in this model [16, 24], the mechanism of the BOLD post-stimulus undershoot has been suggested to be a temporal mismatch between blood flow and volume. In this optical imaging study, [$HbO_2$] adds information that is not directly available from fMRI. Significantly, we note that the temporal profile of [$HbO_2$] shows a post-stimulus undershoot. There are two possible explanations for this. One explanation is that arterial blood volume undershoots the baseline following stimulation, which would contribute to [$HbO_2$] only. Since CBF has been observed to undershoot following stimulation in some models [128], this possibility cannot be discounted.

However, perhaps a more parsimonious explanation is that the transient post-stimulus features of [HbR], [$HbO_2$], and [HbT] are temporally similar because they derive from a common physiological source. It has been postulated that blood volume is elevated only in the venous compartment following stimulation [25]. However, if the capillary compartment shows the same temporal response, this could consistently explain all the optical data. In a diffusion-limited model of oxygen delivery from the blood to brain tissue [70], elevated capillary blood volume provides a mechanism to increase oxygen delivery even if CBF has returned to baseline. Thus, [$HbO_2$] would show a post-stimulus undershoot, [HbT] would show a slow post-stimulus decay due a slow response of both capillary and venous CBV, and the mechanism of the [HbR] overshoot would be attributed to both elevated CBV and an increased rate of oxygen utilization ($CMRO_2$).

### *Dependence on stimulation parameters*

In order to investigate the robustness of the forepaw stimulation paradigm and to illustrate the utility of DOT for functional imaging studies, the hemodynamic effects of various parameters were explored. Figure 6.7 shows the FWHM and peak signal magnitude of [$HbO_2$] (in arbitrary units) vs. stimulus frequency, current, and duration. Since the relative magnitudes of [$HbO_2$] and [HbR] responses were qualitatively similar (albeit opposite in direction), only the [$HbO_2$] response is shown. Each dataset was collected from only two rats, and should be considered as qualitative observations.

The [$HbO_2$] signal magnitude increased sublinearly (i.e. compressed) with increasing stimulus current. If correct, this implies that a saturation in neural activation occurs at a stimulus current near 2mA. In a plot presented by Spenger et. al. [129], the majority of their data shows a similar plateau in response amplitude at ~1.5mA. The FWHM of the hemodynamic response decreased significantly with increasing stimulus current, however the onset delay remained constant. The signal magnitude and FWHM both grew sublinearly with increasing stimulus duration out to 30 seconds.

Signal magnitude decreased in approximate inverse proportion to stimulus frequency. This trend was also observed by Gyngell et. al. and Brinker et. al., who both noted a decrease in T2* fMRI

contrast with increasing stimulus frequency, and attributed it to a progressive reduction in the neuronal recovery time [26, 130]. The FWHM appeared to peak at 3Hz and then decreased in inverse proportion to stimulus frequency. This could result from frequency-sensitive activation of different neural pathways within the cortex, each of which may elicit different hemodynamic responses. Similar research on rat whisker barrel cortex has revealed frequency-selective or "tuned" neural responsivity vs. stimulus frequency, which appeared as a variation in the spatial extent of activation [131]. It is conceivable that a similar frequency-dependent neural activation also occurs during forepaw stimulation, and this might account for our observations. This could also result from habituation, which would cause progressive neuronal attenuation with increasing frequency.

Signal amplitude was also observed to vary with electrode placement (data not shown). Although total stimulus current is easy to quantify, the actual current distribution within the forepaw itself is not easily measured. In future experiments, this aspect will need to be addressed more carefully, perhaps by using monitor electrodes to directly assess the degree of neural activation.

### 6.2.5 Conclusions

Both DOT [HbR] and [$HbO_2$] compared well to fMRI BOLD during stimulation but their profiles differed in the post-stimulus region, which suggests that different hemodynamic mechanisms might be responsible for the post-stimulus responses of the [HbR] and [$HbO_2$] signals. The DOT [HbT] time courses followed the 6 and 30 second fMRI CPV time courses reasonably well. The similarity of the DOT and MRI hemodynamic measures suggests that the vascular sensitivity of the two methods is qualitatively similar, but not identical.